Search for Resonances and New Physics

Nuno T. Leonardo

Laboratório de Instrumentação e Física Experimental de Partículas, Lisbon, Portugal

DOI: http://dx.doi.org/10.3204/DESY-PROC-2016-04/Leonardo

The appearance of new resonances is a most spectacular means by which physics beyond the standard model may be revealed at the LHC. Searches are conducted for bumps in mass spectra exploring a multitude of final states. Results are presented spanning from sub-GeV to multi-TeV scales.

1 Introduction

The Large Hadron Collider (LHC) is currently the world's energy and intensity frontier hadron accelerator, providing collisions at record center-of-mass energies and high luminosities. The LHC along with its detectors is allowing to collect unique datasets of unprecedented size, quality, and potential for physics discovery.

The LHC has completed in early 2013 its first running phase (Run1) and the experiments have collected data sets of proton-proton (pp) collisions at centre-of-mass energies of 7 and 8 TeV with integrated luminosities of about 5 and 20 fb^{-1}, respectively. After an upgrade period for both accelerator and detectors, the second data taking period (Run2) started in mid 2015 at 13TeV, and the experiments had collected already in excess of 15 fb^{-1} at the time the school took place in Dubna. In addition to its main pp programme, the LHC provides collisions involving heavy ions. Valuable datasets of lead-lead (PbPb) and proton-lead (pPb) collisions have been gathered, at centre-of-mass energies per nucleon pair of 2.76 and 5.02 TeV.

Analyses of the collected data have produced a rich set of physics results. These include detailed measurements of a variety of processes, and extensive searches, both indirect and direct, for new particles. The discoveries achieved so far include new particle states and new processes. Among many others these count the observation of a new resonance, compatible with the Higgs boson, and of an ultra-rare process (B_s meson decay into two muons) in pp collisions, and of sequential meson melting of quark-antiquark bound states in PbPb collisions. The results attained in Run1 have lead to the corroboration of the standard model of particle physics (SM) as an extremely successful effective theory and to the exclusion of large, relevant regions of the parameter space available for proposed scenarios extending the SM.

The exploration of the datasets being collected at the new record energy of 13TeV, as well as the ones that will be gathered over the next decades with enhanced accelerator and detectors (the High-Luminosity LHC phase), hold the enormous potential of detecting New Physics, beyond the SM, thus allowing for ground-breaking advancements in our understanding of Nature at the most fundamental level.

2 Detection

The collisions are produced at the center of the detectors – ATLAS, CMS, ALICE and LHCb – that register the debris of the collisions used to reconstruct and study the involved physics processes. ATLAS and CMS are general-purpose detectors, while ALICE and LHCb are specialised in the study of collisions with heavy ions and of processes involving b and c quarks, respectively.

Figure 1 illustrates the particle reconstruction process at CMS. The central feature of the CMS apparatus is a superconducting solenoid of 6m internal diameter, providing a magnetic field of 3.8T. Within the solenoid volume are a silicon pixel and strip tracker, a lead tungstate crystal electromagnetic calorimeter (ECAL), and a brass and scintillator hadron calorimeter (HCAL), each composed of a barrel and two endcap sections. Forward calorimeters extend the pseudorapidity coverage provided by the barrel and endcap detectors. Muons are measured in gas-ionisation detectors embedded in the steel flux-return yoke outside the solenoid.

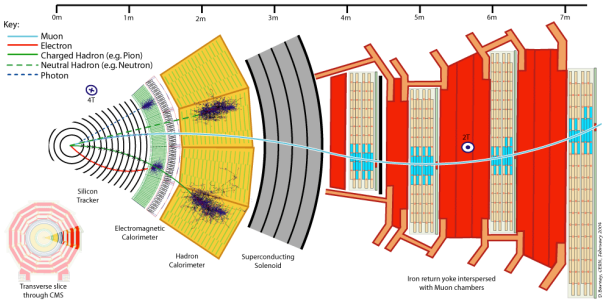

Figure 1: Illustration of particle reconstruction in a general-purpose detector (CMS).

Information from the various elements of the detector is used to reconstruct and identify the stable particles produced in the collisions, by what is dubbed a particle-flow algorithm. The energy of photons is directly obtained from the ECAL measurement, corrected for zero-suppression effects. The energy of electrons is determined from a combination of the electron momentum at the primary interaction vertex as determined by the tracker, the energy of the corresponding ECAL cluster, and the energy sum of all bremsstrahlung photons spatially compatible with originating from the electron track. The energy of muons is obtained from the curvature of the corresponding track. The energy of charged hadrons is determined from a combination of their momentum measured in the tracker and the matching ECAL and HCAL energy deposits, corrected for zero-suppression effects and for the response function of the calorimeters to hadronic showers. Finally, the energy of neutral hadrons is obtained from the corresponding corrected ECAL and HCAL energies. Figure 2 displays reconstructed collision events. In addition to the underlying event, pairs of energetic muon, electron, photon, and jet candidates are featured.

The LHC collisions (bunch crossings) occur at a rate of 40 million times per second. Only a small fraction of which is read out and selected in real time to be recorded for later analysis. The filtering involved is a critical step, and is implemented by a two-tiered trigger system. The first level (L1), composed of custom hardware processors, uses information from the calorimeters and muon detectors to select events at a rate of around 100kHz within a time interval of less than 4μs. The second level, known as the high-level trigger (HLT), consists of a farm of processors running a version of the full event reconstruction software optimised for fast processing, and reduces the event rate to less than 1kHz before data storage.

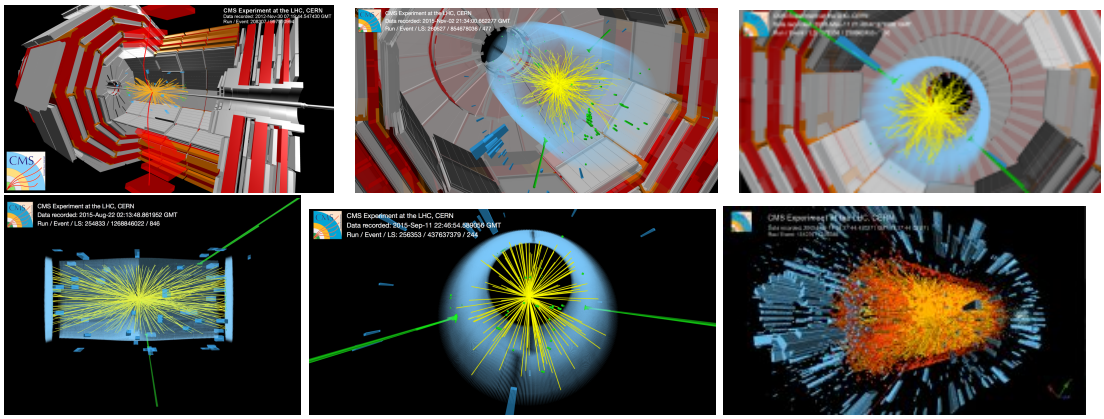

Figure 2: Collision events displaying the following featured candidates (ordered left-to-right, top-to-bottom): di-muon, di-electron, di-photon, di-jet, di-photon with the solenoid turned-off, all in pp collisions, and di-muon in a PbPb collision.

3 Low-mass resonances

Muon signals are cleanly reconstructed, with high accuracy down to low transverse momentum (p_{T}), reaching precisions of 1-2% in the central CMS detector. The probability of misidentifying other particles (hadrons) as muons is low, down to the permill level. Figure 3 displays the di-muon mass spectrum, obtained with data collected in 2016 at 13TeV. It illustrates the ability of the detector to precisely explore a wide-range of particle energies and masses across the spectrum, from the light vector mesons, ω, ϕ, to quarkonia ($J/\psi, \Upsilon$), to the Z^0 vector boson and well beyond it. Note that in order to display the precision achieved across different orders of magnitude, the graph is constructed with a variable width binning in doubly log scales.

Multi-muon signals are explored extensively. Coupled with other particles and vertex-displacement criteria, they form the baseline for online selection of heavy flavors at the general-purpose detectors. In addition to generic, high-p_{T} double-muon trigger algorithms, shown in light gray, Fig. 3 highlights dedicated algorithms, with low-p_{T} thresholds, in specific mass windows.

Quarkonia, heavy quark-antiquark bound states, are extensively explored, forming a laboratory in which to study the strong interaction and, in particular, the mechanisms of hadron production. Precision measurements of produc-

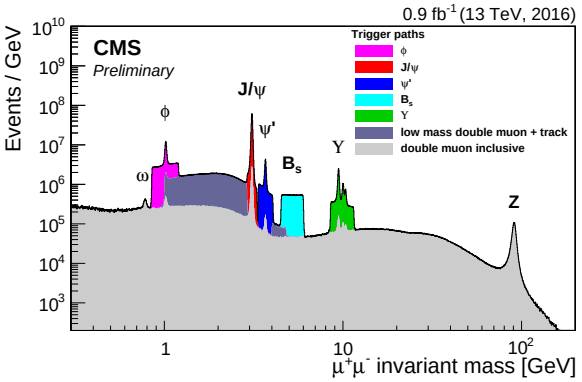

Figure 3: Di-muon mass spectrum.

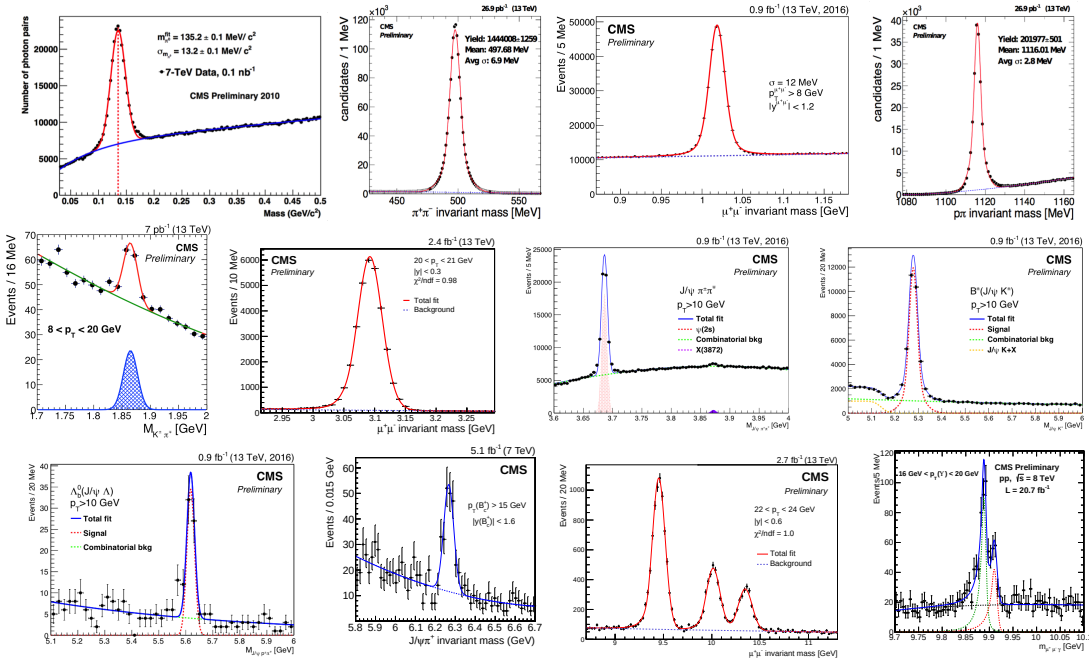

Figure 4: Selected hidden and open flavour resonances, from 0.1 to 10 GeV (ordered from left-to-right, top-to-bottom): π^0, K^0_s, $\phi(1020)$, Λ, D^0, J/ψ, ψ' and X(3872), B^+, Λ^0_b, B^+_c, Υ(nS), χ_b.

tion cross sections and polarisations are performed, which are in turn jointly used to constrain parameters of QCD effective models (e.g. non-relativistic QCD). The properties of hadrons containing b-quarks, identified by their characteristic long lifetimes and corresponding measurable displacement in the detector, are explored in detail which result is high precision tests of

the SM. Figure 4 shows a selection of hadronic signals.

Various final states, involving muons, photons, and light hadrons, are employed to search for new resonant states at low mass. The outcome of these searches includes the first experimental observation of new meson and baryon states, specifically excited states of the χ_b, B_c, or Ξ_b hadrons, as shown in Fig. 5. These observations involve relatively complex decay topologies, of up to six final state particles and four distinct displaced vertices, or low-energy photon conversion to electron-positron pairs in the material of the inner detector.

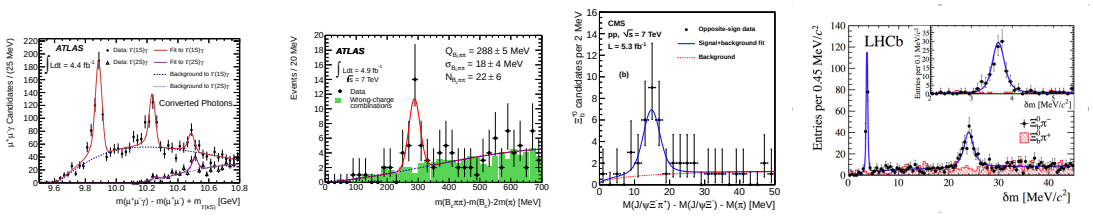

Figure 5: New low-mass resonances (anticipated) (ordered left-to-right): $\chi_b(3P)$; $B_c(2S)$; Ξ_b^{*0}; $\Xi_b^{\prime -}$ and Ξ_b^{*-}.

In addition to searching for structures directly in mass spectra, multi-body final-state hadronic decays are explored to search for new resonant structures in the decay products. For example, the decay $B^+ \to \psi\phi K^+$ is used to explore possible structures in the $\psi\phi$ invariant mass. As displayed in Fig. 6, enhancements in the $J/\psi\phi$ spectrum have been identified by

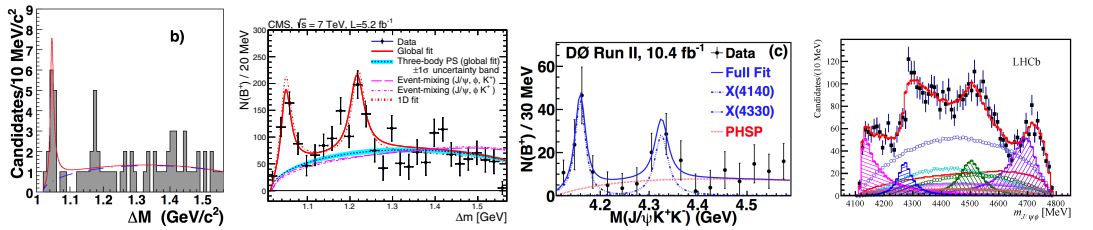

Figure 6: New low-mass resonances (unanticipated). Structures in the $J/\psi\phi$ mass spectra identified at 4.140, 4.274, 4.500, 4.700 GeV.

different experiments, between 4 and 5 GeV. These are unanticipated structures that add to the growing list of candidates for exotic, hadronic particles, which started to be formed with the observation of the X(3872) by Belle more than a decade ago. Further data should allow measurements of their properties and contribute to a clarification of their nature.

The decay process $\Lambda_b^0 \to J/\psi pK$ is explored to tag the $J/\psi p$ final state. A full amplitude analysis of the process achieves a best description of the data, shown in Fig. 7, with the addition of two new states, with masses near 4.4GeV. These new resonances decaying strongly into $J/\psi p$ should have a minimum quark content of $c\bar{c}uud$, thus being hidden-charm pentaquark candidates (labeled P_c^+). The high-yield $B_s^0 \to J/\psi\phi$ channel is explored to search for new, prompt states. Evidence of an excess in the $B_s^0\pi$ invariant mass has been reported, which could be interpreted as an open-beauty tetraquark candidate. However, independent confirmation of the excesses has not been achieved.

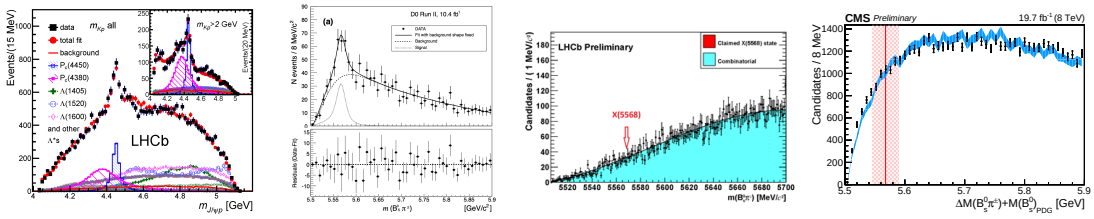

Figure 7: New low-mass resonances (unconfirmed). (leftmost) observation of two pentaquark candidates with masses about 4.4GeV; (others) evidence and search for a tetraquark candidate with mass of about 5.6 GeV.

The complementary study of the strong sector is achieved by exploring collisions involving heavy nuclei. Exclusive measurements of a variety of particle states in heavy-ion collisions have been or will be achieved for the first time at the LHC, which serve as precious hard probes of the hot and dense medium. These include heavy-flavor states, such as b and c quark hadrons, W and Z bosons, and eventually the top quark. Among a large set of unique results achieved, a Run1 highlight is the observation of sequential quarkonium suppression – a spectacular indication of quark-gluon plasma (QGP) formation at the LHC. The relative suppression of the three Υ(nS) states offer sa rare picture of a clear effect in a complex environment – as shown in Fig. 8, not only is each Υ state suppressed in PbPb compared to pp collisions, but the excited states are significantly more suppressed.

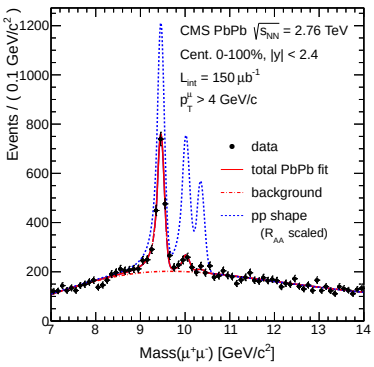

Figure 8: Observation of onia sequential suppression.

The exploration of low-mass spectra in pp collisions involves also the search for new light elementary particles. A search is performed for pair production of new light bosons (a) decaying to pairs of isolated di-muons. One production mechanism for these new bosons is in the decay chain of a Higgs boson (h): $h \to 2a + X \to 4\mu + X$, where X denotes possible additional particles from cascade decays of the Higgs boson. The data mass spectrum is shown in Fig. 9 and does not feature any significant addition beyond the resonance states $\omega, \rho, \phi, \mathrm{J}/\psi$ that are here backgrounds for the analysis. While the search is designed to be model independent, a range of BSM scenarios predict this decay topology, including the next-to-minimal supersymmetric standard model (NMSSM) and models with hidden or dark sectors. Production limits are placed in the context of these benchmark BSM scenarios.

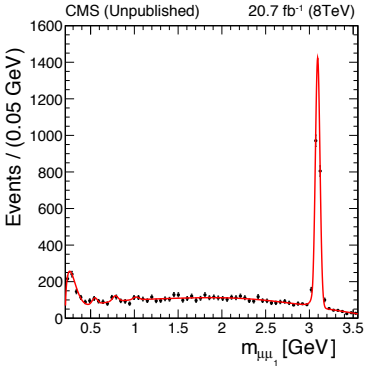

Figure 9: Search for pairs of resonances $h \to 2a \to 4\mu$.

The study of electroweak decays of heavy-flavored hadrons continues to provide stringent SM tests. A class

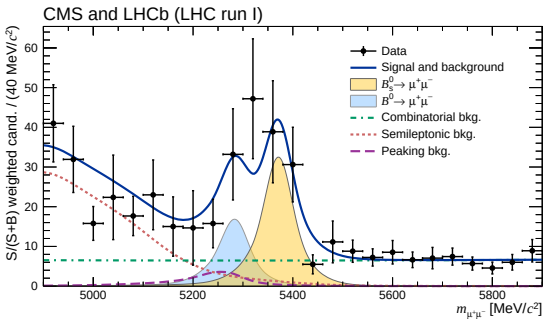

Figure 10: Observation of $B_s^0 \to \mu\mu$.

of processes that is particularly sensitive to BSM effects is provided by rare decays. The study of $B \to K^{(*)}\mu\mu$ decays have resulted in deviations at the 3σ level relative to theory predictions (which are however made challenging due to hadronic form factors). The theoretically clean, ultra-rare processes $B_{(d)}^0 \to \mu\mu$ are extremely suppressed in the SM and therefore particularly sensitive to BSM effects. Their search has spanned about three decades across different experiments in different colliders. SM-level sensitivity is attained only with the LHC. The separate analyses of the Run1 datasets collected by the CMS and LHCb experiments resulted in 4.3σ and 4.0σ evidence for the B_s^0 decay, respectively, while the combined fit to the two datasets, performed by the collaborations and shown in Fig. 10, yielded a significance in excess of 6σ. While the analysis was optimised for the B_s^0 search, an excess was also obtained at the 3σ-level for the B^0 decay, which is however more directly affected by the estimation of the contribution from b-hadron two-body hadronic decays when muons are misidentified that peak in the signal region. The analysis result is compatible with the SM, and exclude vast regions of the parameter space of BSM models. The result is regarded as one of the flagship discoveries of LHC Run1.

4 Intermediate-mass resonances

Isolated leptons allow to reconstruct the SM vector bosons W and Z, across the different collisions energies and systems provided by the LHC, as shown in Fig. 11. These serve as standard

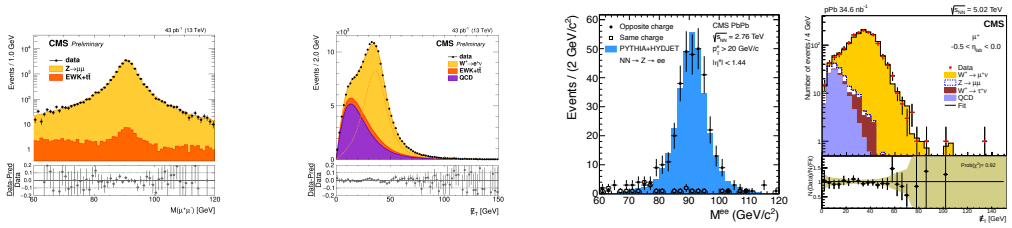

Figure 11: Vector bosons reconstruction. Ordered left-to-right: $Z^0 \to \mu\mu$ and $W^\pm \to e\nu_e$, in pp; $Z^0 \to ee$, in PbPb collisions; $W^\pm \to \mu\nu_\mu$, in pPb collisions.

candles for detector and simulation calibration at high p_T, references for searches of heavier

(BSM) gauge bosons, and as final-state particles in searches for heavier resonances. Precision measurements of production and decay are carried out in pp collisions. The vector bosons have now been observed for the first time also in collisions involving nuclei. They serve as colourless probes that remain unaffected by the hot and dense QCD medium produced, and thus as control for processes expected to be heavily modified in the nuclear media.

One of the original goals of the LHC physics program was the clarification of the electroweak symmetry breaking mechanism. The ATLAS and CMS collaborations first reported the discovery of a new boson in 2012, at a mass of abut 125 GeV. The experimental evidence collected since is consistent with the particle being the Higgs boson, the quantum of the scalar field postulated by the Higgs mechanism. Figure 12 shows the 2-photon and 4-muon mass spectra obtained with recent data, illustrating the boson's re-discovery in Run2. The measurement of the particle's properties with improving precision, also exploring rarer channels, will continue to be pursued with priority with the increasing dataset.

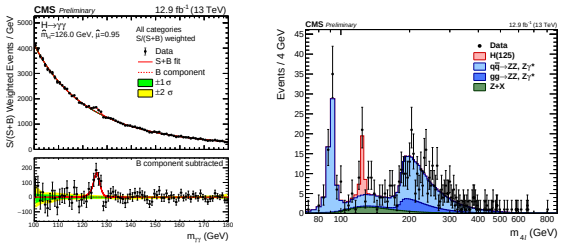

Figure 12: Higgs (LHC Run2) re-discovery.

The new scalar, along with the vector bosons, is explored in the search for BSM effects, via the study of or search for rare or SM-forbidden production and decay modes. The Higgs searches are further extended to higher mass ranges, as also illustrated in Fig. 12 (for the lepton channel). The search for heavier di-photon resonances is similarly explored, as in Fig. 13.

Much excitement was raised by a modest excess at a mass of about 750 GeV in the di-photon data collected in 2015. This raised discussions about possible explanations in terms of new physics and the possible production of a new, BSM particle decaying to two photons. The (local) statistical significance of the excess was between 3σ and 4σ for the ATLAS and CMS experiments, reducing to 2σ and less once the effect of searching under multiple signal hypotheses is considered (global significance). However, at mass and widths corresponding to the largest deviations from the background-only hypothesis in the 2015 data, no large excess is observed in the 2016 data.

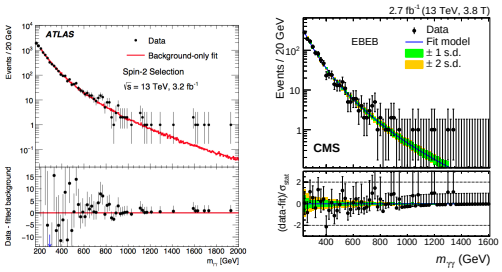

Figure 13: An excess at 750 GeV ?

The main reason for the original 750 GeV excitement was arguably that compatible excesses were detected by two independent experiments in the first place. However, in general, fluctuations at similar level should not come as a surprise – considering the large number of searches for new particles that are performed, we are guaranteed to occasionally see excesses in some regions of some analyses purely from statistical fluctuations of the data.

5 High-mass resonances

The search for massive resonances is pursued similarly in a multitude of ways.

Many BSM models require new particles that couple to quarks and gluons and can be observed as resonances in the di-jet mass spectrum. The spectrum arises from the scattering of partons at high p_T and is predicted by QCD to fall smoothly with increasing di-jet mass. The search for new resonances is pursued in a model-independent way, by inspecting the spectrum shown in Fig. 14, here probed up to 8 TeV, and hunting for bumps. No significant excess is observed and predicted signals from narrow gluon-gluon, quark-gluon, and quark-quark resonances are shown therein with cross sections equal to the observed upper limits at 95% CL.

The di-lepton spectra, shown in Fig. 15 for opposite-sign muons, electrons, muon-electron, and taus, is searched also for high-mass resonance states. No clear, significant excesses above the SM backgrounds are found, and limits are placed on benchmark BSM models.

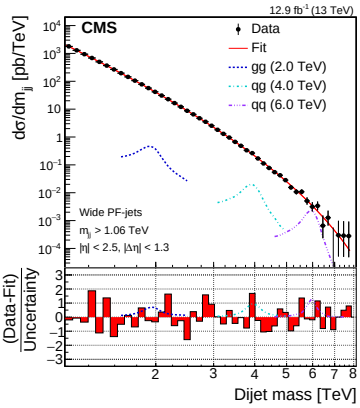

Figure 14: Di-jet spectrum.

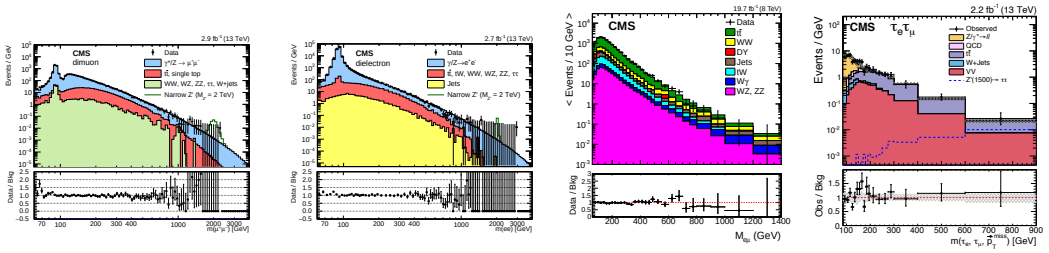

Figure 15: Searches for high-mass resonances in di-lepton spectra: $\mu\mu, ee, \mu e, \tau\tau$.

BSM resonances are searched for also in their decays to di-bosons, including the new scalar (H), as shown in Fig. 16. Sufficiently massive resonances tend to produce highly Lorentz-boosted objects, which yield collimated decay products; when these are partially or fully merged into single jets, methods to analyse jet substructure and suitable jet-tagging techniques are employed.

When no significant excess is observed in the data, exclusion limits on specific benchmark models are placed. Figure 17 provides an overall summary of the exclusion limits achieved in the context of the specified categories of BSM scenarios. The analysis of the 8TeV data and specially of the initial 13TeV data recently collected results in exclusion limits of around several TeV.

6 Exotic resonances

With the goal of 'leaving no stone unturned', searches are performed exploring less conventional signatures. These tend also to often require less orthodox analysis strategies, such as dedicated

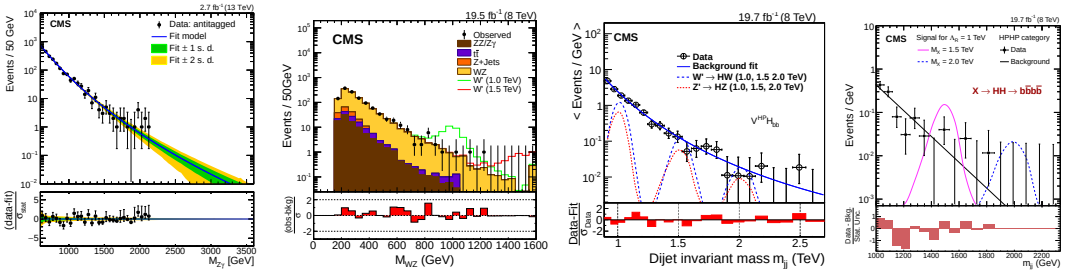

Figure 16: Searches for new, massive resonances in the di-boson spectra: $Z\gamma, WZ, HW, HH$. Specific candidate BSM states are also overlaid, for illustration purposes, which are however not corroborated by the data.

approaches to trigger selection and event processing and reconstruction. One may opt to collect data in a dedicated stream that reads out only selected sub-detector elements instead of the full event (data scouting). One may select events un-asynchronously with the LHC collisions (in between bunch-crossings, in order to collect exotic particles with highly delayed decays). Or search for resonances that, being sufficiently long lived, would have time to travel away from the collision point and decay at a highly displaced vertex – as BSM scenarios such as hidden valleys and stealth or RPV or displaced SUSY among others would have it. The exclusion limits are summarised in Fig. 17 also for some of these more exotic scenarios.

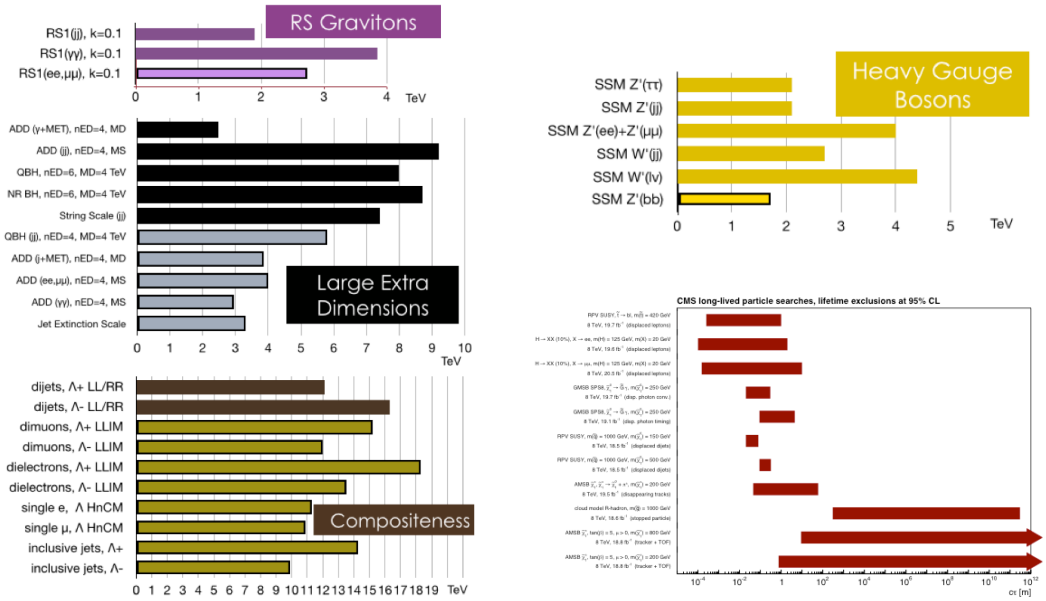

Figure 17: Summary of current 95% CL upper exclusion limits on the mass of new resonances in various BSM scenarios.

7 Conclusion

The LHC and its detectors have had an extremely successful first running period, and are initiating its second data-taking period at higher collision energies. Various new resonances – both anticipated and unexpected – have been discovered. In addition, new processes and phenomena have been observed, and old ones probed to unprecedented precision. The standard model has in the process been reinforced as an extremely successful effective theory. The bulk of the LHC data that will be gathered over the coming years and decade carry the promise and potential of detecting what physics lies beyond it – the overarching goal we pursue.

Acknowlegements:
The author acknowledges support by grants FCT IF/01454/2013/CP1172/CT0003 and CERN/FP/123601/2011, Portugal. He wishes to thank the organisers for the Lecture invitation and the wonderful gathering in Dubna.

General references

[1] ATLAS Collaboration public results,
`https://twiki.cern.ch/twiki/bin/view/AtlasPublic`

[2] CDF Collaboration public results,
`https://www-cdf.fnal.gov/physics/physics.html`

[3] CMS Collaboration public results,
`http://cms-results.web.cern.ch/cms-results/public-results/publications/`

[4] D∅ Collaboration public results,
`http://www-d0.fnal.gov/d0_publications`

[5] LHCb Collaboration public results,
`http://lhcbproject.web.cern.ch/lhcbproject/Publications/LHCbProjectPublic/Summary_all.html`